

One-pot synthesis of magnetic, macro/mesoporous bioactive glasses for bone tissue engineering

Dan Wang, Huiming Lin, Jingjie Jiang, Xiao Han, Wei Guo, Xiaodan Wu, Yingxue Jin and Fengyu Qu¹

State Key Laboratory of Photoelectric Band Gap Materials, College of Chemistry and Chemical Engineering, Harbin Normal University, Harbin, People's Republic of China

E-mail: qufengyu@chem@yahoo.com.cn and huiminglin@gmail.com

Received 21 December 2012

Accepted for publication 21 March 2013


Published 19 April 2013

Online at stacks.iop.org/STAM/14/025004

Abstract

Magnetic and macro/mesoporous bioactive glasses were synthesized by a one-pot method via a handy salt leaching technique. It was identified to be an effective and simple synthetic strategy. The non-ionic triblock copolymer, poly(ethylene glycol)-block-poly(propylene glycol)-block-poly(ethylene glycol) (P123), was used as the structure directing agent for mesoporous structure but also as the reductant to reduce the iron source into magnetic iron oxide. The prepared materials exhibited excellent super-paramagnetic property with interconnected macroporous (200–300 μm) and mesoporous (3.4 nm) structure. Furthermore, their outstanding drug storage/release properties and rapid (5) induction of hydroxyapatite growth ability were investigated after immersing in simulated body fluid solution at 37 °C. Notably, the biocompatibility assessment confirmed that the materials obtained presented good biocompatibility and enhanced adherence of HeLa cells. Herein, the novel materials are expected to have potential application for bone tissue engineering.

Keywords: magnetic, porous, bioactive glasses, drug delivery, bone tissue engineering

 Online supplementary data available from stacks.iop.org/STAM/14/025004/mmedia

1. Introduction

Nowadays, bone defects due to bone trauma and osteocarcinoma represent a major challenge and global health problem [1, 2]. Since the early years, autografts have been considered as the 'Gold Standard' in oral surgery and implant dentistry because of the best regenerating results they provide. However, due to the problems associated with secondary trauma and generation of immune repulsion, the

availability of autografts for bone regeneration engineering is limited. Other methods such as bone allografts and synthetic graft materials are often used as alternatives [3, 4].

In the last several years, three types of synthetic bone substitution materials have been developed: metallic [5], polymeric [6] and ceramic implants [7]. With high mechanical strength and forgeable properties, metallic materials are employed as bone substitutes. However, toxic ions (heavy metal ions) spread inside the body from such materials, which restrict their wide application for bone substitution and regeneration [8]. Polymeric materials possess a similar elastic modulus to bone, but their applications are hampered by inferior biocompatibility and bioactivity [9]. Because of the good biocompatibility, hardness and chemical stability,

¹ Author to whom any correspondence should be addressed.



Content from this work may be used under the terms of the Creative Commons Attribution-NonCommercial-ShareAlike 3.0 licence. Any further distribution of this work must maintain attribution to the author(s) and the title of the work, journal citation and DOI.

ceramic materials are deemed to be potential candidates for skeletal repair and substitution materials. In particular, the design of multifunctional ceramic implants for bone regeneration and therapy in bone surgery has attracted most attention [10].

Since the 1970s, much attention has been paid to bioactive glasses (BGs) [11], an important ceramic material. Based on the excellent biocompatibility, osteoinductivity and osteoconductivity, BGs [12, 13] are thought to be suitable materials for bone replacement. Based on recent reports, the interconnected network (200–300 μm) is conducive to growth of tissue/cells and transport of large molecular nutrients [14, 15], and the mesoporous structure promotes the adsorption and release of biological metabolites at controlled rates to match the demand of tissue repair [16].

Magnetic materials were widely used in biopharmaceutical fields as magnetic targets [17] and magnetic resonance imaging reagents [18, 19]. Moreover, the magnetic nanoparticles can produce localized hyperthermia by hysteresis heating upon exposure to an alternating magnetic field [20]. When the temperature is raised to 42–45 °C, tumor/cancer cells are damaged or killed due to overheating, while most of the normal cells survive [21, 22].

As we all know, most of the typical methods to synthesize magnetic materials need a reducing atmosphere (H_2) to reduce the iron source to magnetic iron oxide [23, 24]. The preparation process is insecure and the cost is expensive. However, Pedro [25] and his co-workers have shown that ethylene glycol can be utilized as the reductant to reduce the iron source into magnetic iron oxide depending on the reducing aldehyde, which is derived from thermal decomposition of ethylene glycol. The whole process was conducted in a N_2 atmosphere. In this paper, we use a one-pot method to synthesize magnetic, macro/mesoporous bioactive glasses (MMBGs). The non-ionic triblock copolymer, poly(ethylene glycol)-block-poly(propylene glycol)-block-poly(ethylene glycol) (P123), is used as the mesoporous template. Considering the similarity between ethylene glycol and P123, we try to treat the mesoporous template P123 as the reductant to reduce the iron source as well. When the thermal decomposition of P123 takes place to produce reducing carbon, the iron source is then reduced to magnetic iron oxide. In addition, the organic materials are always replicated as macroporous templates [26, 27] and calcinations in air are needed to produce the macroporous structure. In our work, considering the particularity of the synthetic system, the utilization of organic materials is not permitted because the magnetic iron oxide cannot be transformed in air. Hence, the simple salt leaching processing technique [28], through the filtration of the suitable salt crystal as the macroporous templates, is used to obtain the macroporous structure. Simultaneously, the drug storage/release and biomineralization properties *in vitro* as well as the biocompatibility assessment are studied in detail.

2. Experimental

2.1. Chemicals

All chemicals were of analytic reagent grade and used without further purification. $\text{EO}_{20}\text{PO}_{70}\text{EO}_{20}$ (P123, M_w : 5800) was purchased from Sigma-Aldrich Chemical Company. Tetraethoxysilane (TEOS), triethyl phosphate (TEP), $\text{Ca}(\text{NO}_3)_2 \cdot 4\text{H}_2\text{O}$ and $\text{Fe}(\text{NO}_3)_3 \cdot 9\text{H}_2\text{O}$ were purchased from Tianjin Reagent Company. Hydrochloric acid and ethanol were purchased from Beijing Reagent Company. Sodium chloride (NaCl) was supplied by Shanghai Reagent Company. Ibuprofen (IBU) was obtained from Tianzunzhong Chemical Company.

HeLa cells were applied for subsequent adhesion assays. Dulbecco's phosphate buffered solution, Dulbecco's modified Eagle medium (DMEM)/Ham's F-12 (1:1), penicillin/streptomycin (P/S) and foetal bovine serum (FBS) were purchased from Sigma-Aldrich. The culture medium was prepared as DMEM/Ham's F-12 (1:1) with 10% FBS, 1% P/S and 2 mg l^{-1} of L-glutamine.

2.2. Characterization

The morphologies of the prepared samples were characterized using a scanning electron microscope (SEM, Hitachi S4800) at an accelerating voltage of 20 kV, and sample elements were analyzed by an energy dispersive spectrometer (EDS), associated with SEM. Powder x-ray diffraction (XRD) data were collected on a Bruker D8 ADVANCE diffractometer at 40 kV and 30 mA, using $\text{Cu K}\alpha$ radiation. The specific surface area of samples was determined using Brunauer–Emmett–Teller (BET) (NOVA 4200E Surface Area and Pore Size Analyzer, Quantachrome, USA). The pore size distributions were calculated from the adsorption branches of the N_2 adsorption isotherms using the Barrett–Joyner–Halenda (BJH) model. The magnetic properties of samples were characterized with a Vibrating Sample Magnetometer (Lake Shore 7410). Fourier transform infrared (FTIR) spectra were recorded on a Perkin–Elmer 580B Infrared Spectrophotometer using the KBr pellet technique. The UV–vis absorbance spectra were measured using a Shimadzu UV-3101PC spectroscope. Thermo-gravimetric analysis (TGA) was carried out (Perkin–Elmer Diamond 6300) in a flowing air atmosphere at a heating rate of 10 °C min^{-1} . Transmission electron microscopy (TEM) images were recorded on an FEI Tecnai F20 instrument.

2.3. Preparation of the magnetic, mesoporous bioglasses precursor (MMBGs-p)

The bioglasses (BGs) precursor was prepared by a route of self-assembly of Ca, P, Si and Fe sources in the sol–gel process. In a typical procedure, 4.0 g of P123 was added to 60 g of ethanol under magnetic stirring for 2 h and a transparent solution was obtained. Then, 6.7 g of TEOS, 0.73 g of TEP, 1.40 g of $\text{Ca}(\text{NO}_3)_2 \cdot 4\text{H}_2\text{O}$, 1.0 g of

0.5 M hydrochloric acid and $\text{Fe}(\text{NO}_3)_3 \cdot 9\text{H}_2\text{O}$ were added successively. The molar ratio of MMBGs and Fe was 4:1. The mixture solution was stirred for 24 h.

2.4. Preparation of magnetic, macro/mesoporous bioglasses (MMBGs)

Before the experiment, NaCl crystals (200–300 μm) were calcined at 600 °C for 5 h in an air atmosphere. The macroporous scaffold of MMBGs was prepared depending on salt-leaching techniques. Briefly, the prepared precursor was stepwise dropped on the surface and the gap of the NaCl monolith. Later, the yellow NaCl monolith obtained was dried under vacuum for 40 min at room temperature to evaporate the solvent completely. The same procedure was repeated several times. Then, the monolith was calcined at 350 °C in an air atmosphere for 50, 70, 90 and 110 min, and for 3 h in a N_2 atmosphere at the same temperature. Finally, it was rinsed with distilled water for leaching the salt several times. All samples were named as MMBGs1 (50 min in air), MMBGs2 (70 min in air), MMBGs3 (90 min in air) and MMBGs4 (110 min in air), respectively. The formation process of magnetic, macro/mesoporous bioactive glasses is illustrated in figure 1.

2.5. Drug loading and release

In order to investigate the drug loading of the samples, IBU, a typical anti-inflammatory drug, was used as the model drug. Typically, the experiment was performed as follows: 0.206 g of MMBGs was added to 10 ml of hexane solution with an IBU concentration of 20.6 mg ml^{-1} at room temperature. Then, the mixtures were stirred for 4 h. The IBU-loaded samples were separated by centrifugation and dried under vacuum at 60 °C. The amount of loading IBU was analyzed by UV–vis spectroscopy at a wavelength of 220 nm. The amount of IBU loading was calculated as the amount of IBU loading (%) = $C_{\text{loading}}/C_{(\text{loading}+\text{MMBGs})}$, according to the standard curve of IBU in hexane solution: $y = 0.0194x + 0.0644$, where y is the absorbance and x is the concentration ($\mu\text{g ml}^{-1}$).

Briefly, the IBU-loaded samples were immersed in a beaker with 300 ml of simulated body fluid (SBF) solution. The beaker was incubated at 37 °C in a thermostat shaker. At appropriate intervals, the release medium (3.0 ml) SBF solution was taken and immediately replaced with an equal volume of fresh SBF. The 3.0 ml extracted medium was diluted with SBF solution, and the amount of released IBU in the taken SBF solution was measured by a UV–vis spectrophotometer at 220 nm.

2.6. In vitro biomineralization of MMBGs

The assessment of the *in vitro* biomineralization of MMBGs was conducted in the SBF, which has an ionic composition similar to that of human blood plasma. Each specimen was immersed in 300 ml SBF solution at 37 °C to monitor the formation of hydroxyapatite (HAP) over time. The immersed samples were then taken out from the SBF solution and

washed three times with acetone and ethanol. The resulting samples were analyzed using SEM, EDS, XRD and FTIR.

2.7. Cell adherence

HeLa cells were cultured in culture media at 37 °C in 10% fetal calf serum, 88% (v/v) DMEM, 1% L-glutamine and 1% P/S. The cells were suspended in fresh culture medium and were counted using a Countess cell counting chamber slide in a Countess automated cell counter. The cell suspension was diluted to the required concentration using fresh culture media, so that each scaffold was subsequently seeded with a 40 μl cell suspension containing 10 000 cells.

The cell-seeded scaffolds were incubated for 1 h, before adding 1 ml of culture medium to each well of the 48-well plates. They were further cultured in the incubator for 3 days and the culture medium was renewed once in 2 days.

Specimens were fixed in 2.5% glutaraldehyde in 0.01 M sodium cacodylate buffer (pH 7.3) at 4 °C overnight then dehydrated in a graded series of alcohols (50, 70, 90 and two changes of 100% ethanol), washed with hexamethyldisilazane for 1 min and stored in a desiccator. Then, samples were sputter coated with gold before being examined under a SEM. Observation using the SEM was conducted at an accelerating voltage of 15 kV.

3. Results and discussion

3.1. Structural features

The morphology of MMBGs is shown in figure 2(a). The SEM images demonstrate the three-dimensional interconnected macroporous structure with a pore size of 200–300 μm , which indicates that the salt crystal structure was replicated perfectly. It is worth noting that the pore dimensions within the range of 200–300 μm are suitable for cell attachment, proliferation and migration [29]. The EDS analysis of MMBGs (figure 2(b)) indicates that these samples are only composed of Si, Ca, P, O and Fe. No other hetero-atoms are presented, which shows that the chemical compositions of the final products have been preserved from the precursor solution.

The low-angle XRD patterns of MMBGs1, MMBGs2, MMBGs3 and MMBGs4 are shown in figure 3(a). As is seen, MMBGs2, MMBGs3 and MMBGs4 present an apparent characteristic diffraction peak at $2\theta = 1.12^\circ$, which proves that the mesoporous structures of the samples were formed. In contrast, no diffraction peaks can be observed for MMBGs1, testifying that the calcination time in air is significant for the removal of P123. The shorter calcination time in air induces more P123 residual that is not beneficial for the ordered structure in the final sample. In order to investigate the amount of residual P123, TGA was carried out (supplementary figure S1, available from stacks.iop.org/STAM/14/025004/mmedia). The weight loss between 300 and 500 °C can respond to the residual P123. From MMBGs1 to MMBGs4, the amount of residual P123 is 9, 6, 4 and 2%, suggesting that the shorter the time for calcination in air, the more residual P123 is left. But, as reported [30–33], carbon can be used in the biomedical field and cytotoxicity cannot be found in materials

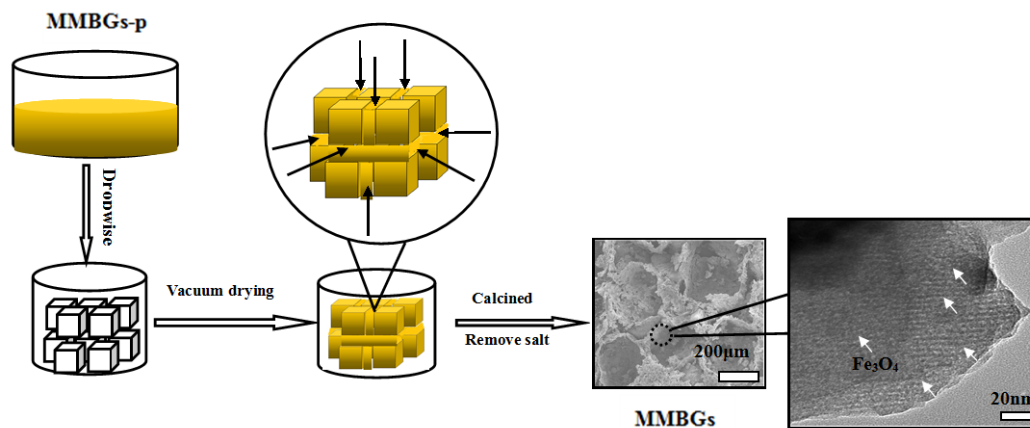


Figure 1. Illustration of the formation process of magnetic, macro/mesoporous bioglasses.

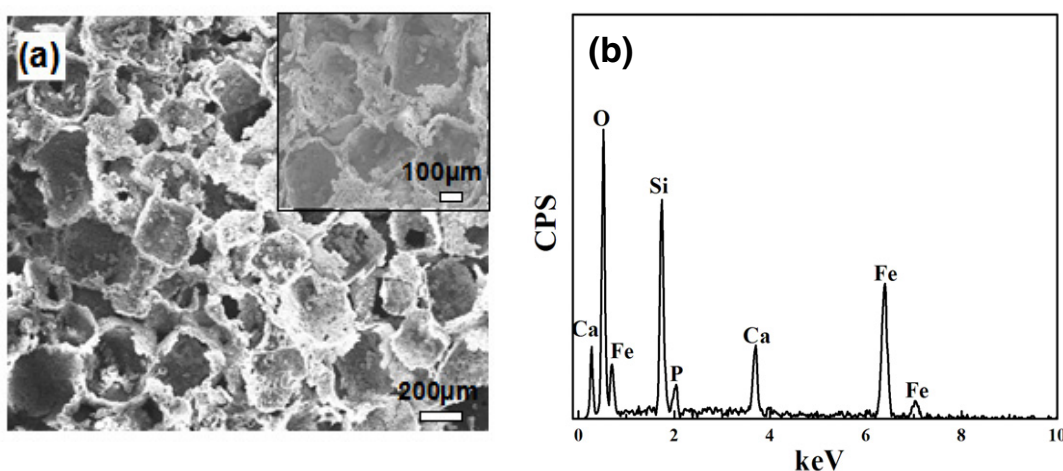


Figure 2. SEM image (a) and EDS analysis (b) of MMBGs.

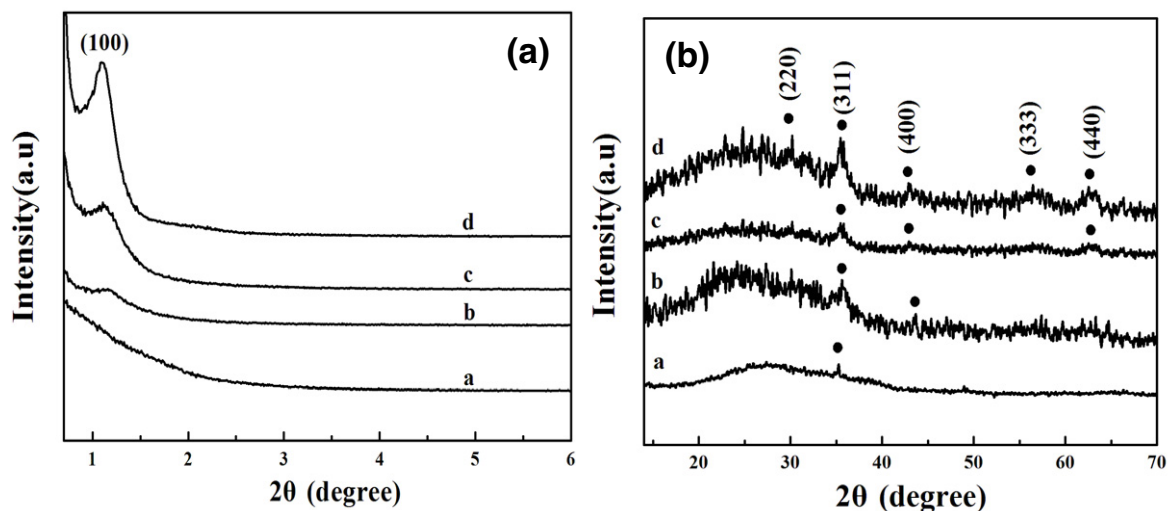


Figure 3. Low-angle XRD patterns and wide-angle XRD patterns of MMBGs1 (a), MMBGs2 (b), MMBGs3 (c) and MMBGs4 (d).

with a low content. Figure 3(b) shows the wide-angle XRD patterns of the samples. A broad peak between 20° and 30° can be clearly observed, which can be ascribed to amorphous silica in all samples. The peaks at 30.1, 35.4, 43.1, 57 and 62.5° correspond to the (220), (311), (400), (333) and

(440) reflection of the typical diffraction of Fe₃O₄ (JCPDS no 79-0416), testifying that Fe(NO₃)₃ can be completely transformed into magnetic iron oxide. Nonetheless, from MMBGs1 to MMBGs4, the characteristic diffraction peaks of Fe₃O₄ become obvious. With a longer calcination time in air,

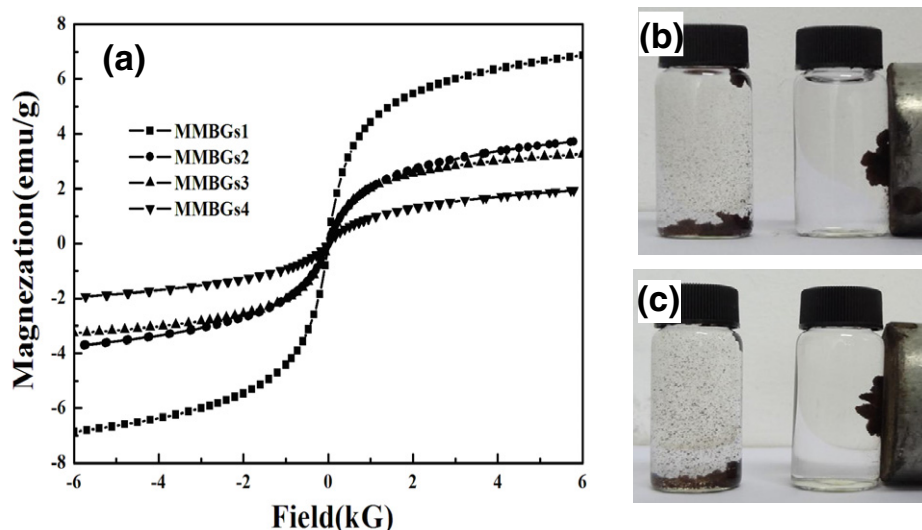


Figure 4. Magnetization curves of four samples at room temperature (a); photograph of dispersed MMBGs2 and MMBGs3 (b), (c) in water before and after being placed near an external magnet.

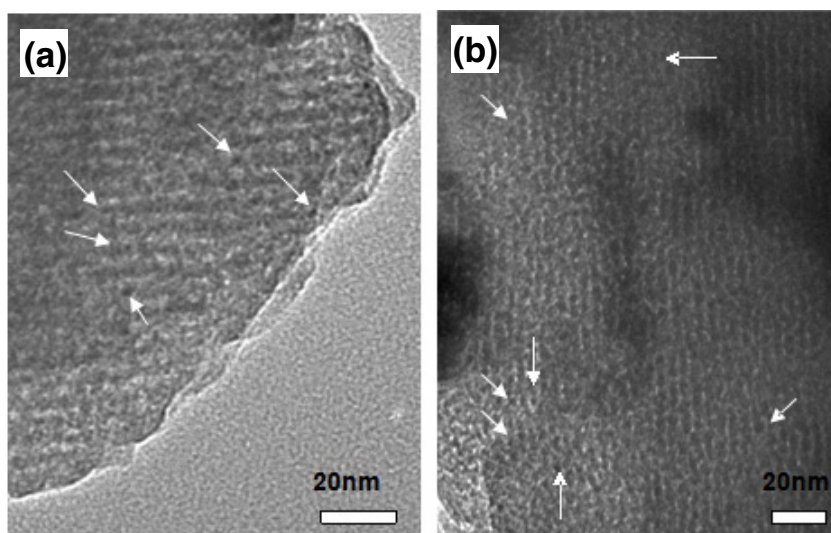


Figure 5. Representative TEM image of the as-synthesized MMBGs2 and MMBGs3. (The arrows indicate the presence of Fe₃O₄ nanoparticles.)

less P123 is left to reduce the iron source and produce less magnetic iron oxide.

To further testify to the correlation of the calcination time in air with the formation of magnetic iron oxide, the magnetic properties of the samples obtained were investigated. Figure 4 presents the magnetization characterization of MMBGs1, MMBGs2, MMBGs3 and MMBGs4 at room temperature. The hysteresis loops (figure 4(a)) indicate the super-paramagnetism of the materials obtained. In addition, the corresponding saturation magnetizations (M_s) of four samples are 6.78, 3.72, 3.19 and 1.96 emu g⁻¹, respectively. The magnetic separability of MMBGs2 and MMBG3 is demonstrated in distilled water by placing a magnet beside the glass bottle. The samples show a fast separating process in 30s when a magnet is placed near the glass bottle (figure 4(b)). By extending the calcining time in air, the saturation magnetization values decrease.

In this synthetic process, residual P123 is used as the reductant, which can reduce Fe³⁺ to Fe₃O₄ depending on the thermal decomposition of P123. The shorter calcining time in air retains more residual P123, which is beneficial to the formation of Fe₃O₄ and induces large saturation magnetization values. From the above investigation, with the good porous structure and magnetic property, MMBGs2 and MMBG3 were selected as suitable materials for bone tissue regeneration.

Figure 5 shows the representative TEM images of MMBGs2 and MMBGs3. All samples show ordered mesoporous structure with a straight channel. Small Fe₃O₄ nanoparticles are homogeneously dispersed in the wall of the matrix and no accumulation of Fe₃O₄ particles can be found, obviously. Nevertheless, compared with the common mesoporous bioglass [34], the ordered degree of mesoporous structure decreases for MMBGs, that is, the assembly of

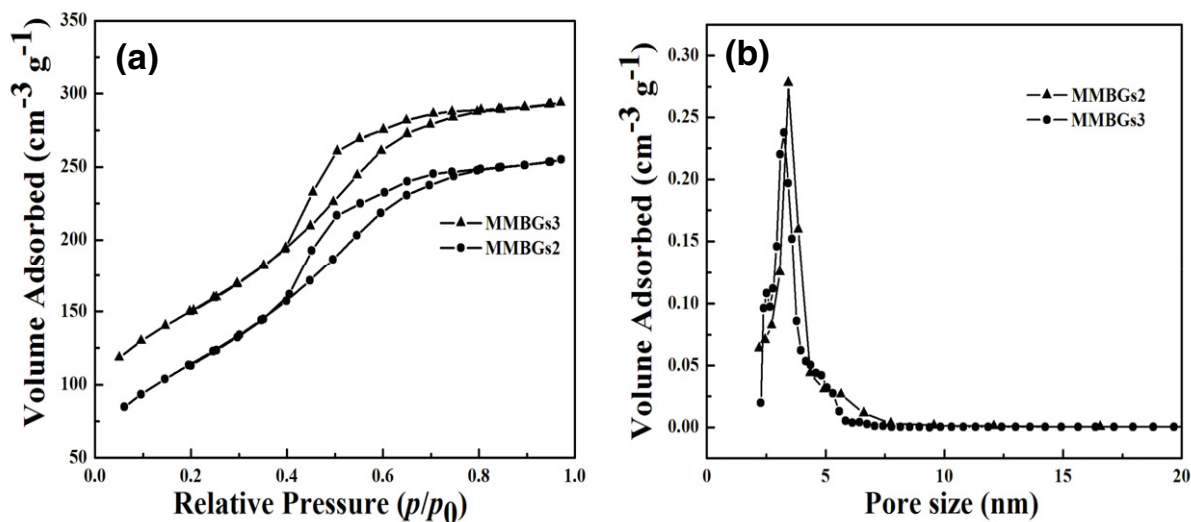


Figure 6. N₂ adsorption–desorption isotherms (a) and BJH-pore distribution (b) of MMBGs2 and MMBGs3.

Table 1. Mesopore pore structure parameters, saturation magnetization values and IBU loading of MMBGs2 and MMBGs3.

Sample	S_{BET} ($m^2 g^{-1}$)	V_p ($cm^3 g^{-1}$)	D_p (nm)	M_v ($emu g^{-1}$)	IBU loading (%)
MMBG2	410	0.386	3.4	3.72	16.4
MMBG3	422	0.378	3.4	3.19	18.7

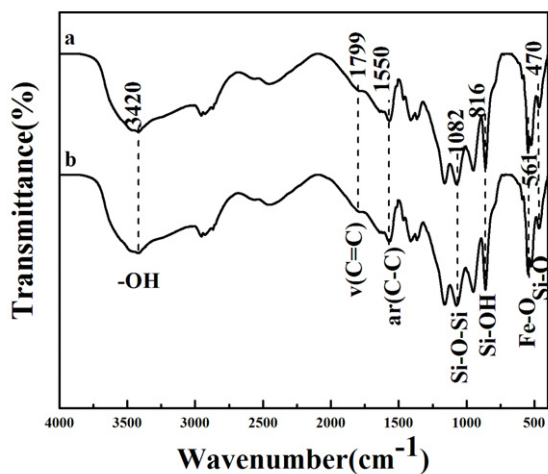


Figure 7. FTIR spectra of IBU-containing materials: MMBGs2 (a) and MMBGs3 (b).

surfactant could be affected by the doping Fe³⁺ to some extent.

Nitrogen adsorption–desorption isotherms are presented in figure 6(a). MMBGs2 and MMBGs3 show the typical IV isotherm curves with a capillary condensation step in the relative pressure range of 0.4–0.6 P/P_0 , suggesting cylindrical mesoporous structure formation. The BJH-pore-size distributions (D_p) show a peak center at 3.4 nm (figure 6(b)). The BET surface areas (S_{BET}) and pore volumes (V_p) of MMBGs2 and MMBGs3 are 422 $m^2 g^{-1}$ and 0.378 $cm^3 g^{-1}$, 410 $m^2 g^{-1}$ and 0.386 $cm^3 g^{-1}$, respectively

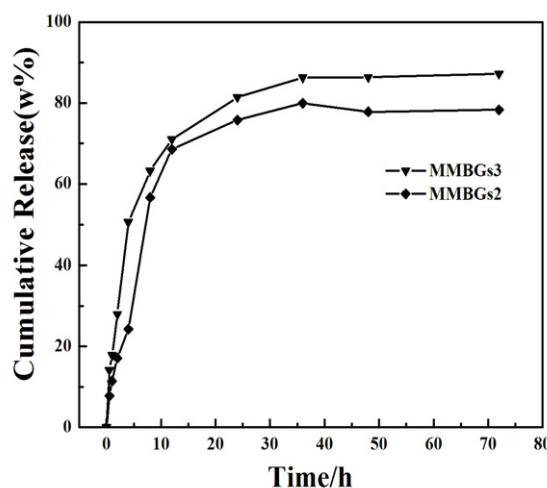


Figure 8. IBU cumulative release of MMBGs2 and MMBGs3 in SBF solution.

(table 1). From the above investigation, the residual surfactant of MMBGs2 is more than that of MMBGs3, making the surface area and the pore volume decrease.

3.2. IBU loading and release

The IBU-loading capacity is shown in table 1. With larger surface area and higher pore volume, MMBGs3 (18.7%) has more outstanding drug-loading capacity than MMBGs2 (16.4%).

The FTIR spectra of MMBGs2 and MMBGs3 are studied to confirm the loading of IBU. From figure 7, the absorption bands of –OH (3420 cm^{-1}), Si–O–Si (1082 cm^{-1}), Si–OH (816 cm^{-1}) and Si–O (470 cm^{-1}) are obvious, indicating the amorphous silica framework formation. The band of Fe–O (561 cm^{-1}) can be attributed to magnetic iron oxide. Moreover, the characteristic bands at 1799 and 1550 cm^{-1} are ascribed to stretching vibration C=O and skeletal vibration of the aromatic ring of IBU, confirming that IBU are successfully loaded into the mesoporous materials.

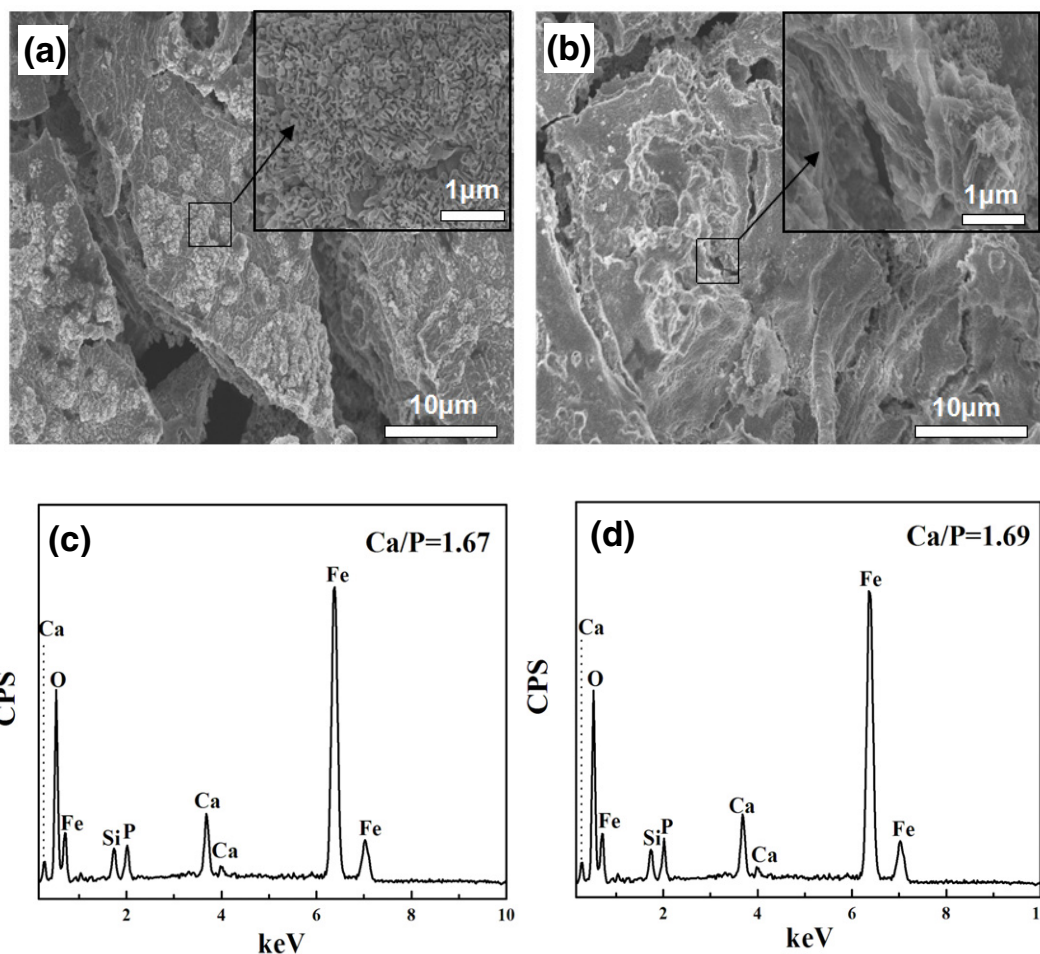


Figure 9. SEM images of the samples: low-resolution image (a), (the inset) high-resolution image of MMBGs2, low-resolution image (b), (the inset) high-resolution image of MMBGs3, EDS patterns of MMBGs2 (c), EDS patterns of MMBGs3 (d) after soaking in SBF for 3 days.

In vitro release experiments of IBU-loaded samples were carried out in SBF, as given in figure 8. The drug release of IBU can be classified into two stages: the drug burst release and the controlled release process. In the first hour, the mean values of IBU release percentages for MMBGs2 and MMBGs3 are 11.4 and 17.8%, respectively. For the initial fast release of IBU, it may be attributed to rapid diffusion of the drug from the macroporous structure. Then, the controlled release takes place at 10h and the cumulative release percentages are 60 and 67%. The drug stored in mesoporous channels diffuses to the macropore after the longer-time penetration of the medium and shows the well-controlled drug release process. Afterwards, at 36 h, the maximal value of the IBU cumulative release percentages of two samples can be obtained as about 80 and 89%.

3.3. Bioactivity of inducing hydroxyapatite (HAP) growth

The HAP inducing-growth ability of the samples was investigated after soaking in SBF at 37 °C for 3 days. From figures 9(a) and (b), the abundant flower-like crystals covering the surface of the samples can be observed. From the further amplification images, all plate-like nanocrystals

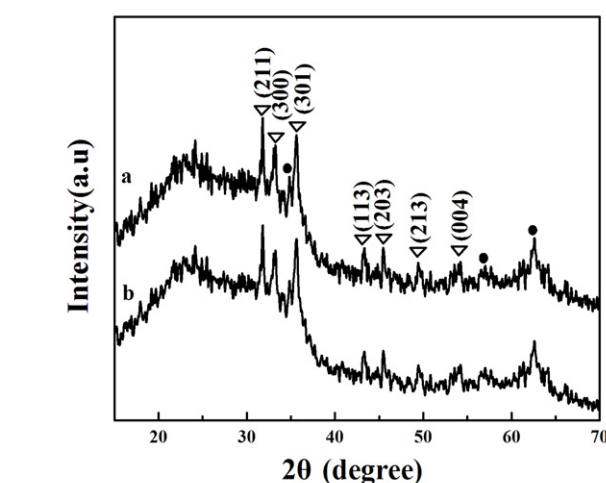


Figure 10. Wide-angle XRD patterns of MMBGs2 (a) and MMBGs3 (b) after soaking in SBF for 3 days. (The circle represents the Fe₃O₄ characteristic diffraction peak; the triangle represents the HAP characteristic diffraction peak.)

are assembled into the flower-like crystals. The corresponding EDS patterns of MMBGs2 and MMBGs3 (figures 9(c) and (d)) demonstrate that the main contents of the samples are

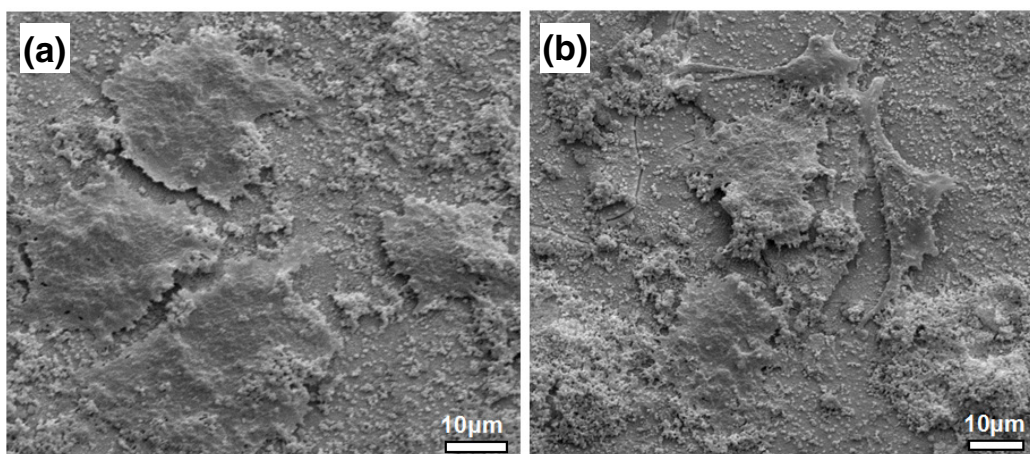


Figure 11. SEM images of HeLa cells morphology onto each surface of MMBGs2 (a) and MMBGs3 (b) after culturing for 3 days.

Si, Ca and P. Additionally, the ratios of Ca/P for formed flower-like crystals are 1.67 and 1.69, respectively. These are consistent with the composition of HAP, proving that these materials can induce the growth of HAP.

Supplementary figure S2 (available from stacks.iop.org/STAM/14/025004/mmedia) represents the FTIR spectra of MMBGs2 and MMBGs3 after soaking in SBF for 3 days. It is certain that the absorption bands of the phosphate groups at 601 and 558 cm^{-1} are from HAP. That further testifies to the growth of HAP [35, 36].

Figure 10 shows the wide-angle XRD patterns of MMBGs2 and MMBGs3 after soaking in SBF for 3 days. The diffraction peaks appearing at 31.8, 33.0, 35.5, 43.8, 45.3, 49.4 and 53.1° can be assigned to the (211), (300), (301), (113), (203), (213) and (004) crystal planes of HAP (JCPDS no. 09-0432). Thus, it further confirms the growth of HAP nanocrystal on the surface of prepared materials by the one-pot method. It is known that HAP is the main inorganic component of human bone. The spontaneous inorganic mineralization of HAP gives these materials potential application in bone tissue regeneration.

3.4. HeLa cell adherence

The SEM images of cells attached onto each surface after incubation for 3 days are displayed in figure 11. All images show that the cells can attach and spread on the surface, suggesting the good biocompatibility and cell adhesion of synthetic materials. This is an important requirement for bone regeneration application.

4. Conclusions

Magnetic and macro/mesoporous bioactive glasses (MMBGs) were successfully synthesized by a novel one-pot method. A simple salt leaching processing technique was used to produce macroporous structure. P123 was used as the mesoporous template and as the reductant to reduce Fe^{3+} to Fe_3O_4 by the thermal decomposition product of P123. It was a simple and feasible way to synthesize the MMBGs. The materials showed

interconnected macroporous (200–300 μm) and mesoporous (3.4 nm) structure, which benefits bone regeneration and drug release. Rapid induced HAP precipitation after immersing in SBF solution indicated the high bioactivity of these materials. Moreover, the cell experiment confirmed that the materials obtained had good biocompatibility and cell adherence ability. With the novel hierarchical porous structure and magnetic property, these materials exhibited potential applications in bone substitution or regeneration.

Acknowledgments

Financial support for this study was provided by the National Natural Science Foundation of China (21171045, 21101046), the Natural Science Foundation of Heilongjiang Province of China (ZD201214, B200913), Program for Scientific and Technological Innovation team construction in Universities of Heilongjiang province (2011TD010), the Research Fund for the Doctoral Program of Higher Education of China (20102329110002) and the Foundation of Harbin Educational Committee (12521164).

References

- [1] Arvidson K, Abdallah B M, Applegate L A, Baldini N, Cenni E, Gomez-Barrena E and Granchi D 2011 *J. Cell. Mol. Med.* **15** 718
- [2] Jiang P P, Lin H M, Xing R and Qu F Y 2012 *J. Sol–Gel Sci. Technol.* **61** 421
- [3] Parikh S N 2002 *J. Postgrad. Med.* **48** 142
- [4] Salgado A J, Coutinho O P and Reis R L 2004 *Macromol. Biosci.* **4** 743
- [5] Alvarez K and Nakajima H 2009 *Materials* **2** 790
- [6] Gentsch R, Pippig F, Schmidt S and Börner H G 2011 *Macromolecules* **44** 453
- [7] Oh S, Oh N, Appleford M and Ong J L 2006 *Am. J. Biochem. Biotechnol.* **2** 49
- [8] Wang M 2003 *Biomaterials* **24** 2133
- [9] Sabir M I, Xu X X and Li L 2009 *J. Mater. Sci.* **44** 5713
- [10] Valllet-Regí M and Ruiz-Hernández E 2011 *Adv. Mater.* **23** 5177
- [11] Rahaman M N, Day D E, Bal B S, Qian F, Jung S B, Bonewald L F and Tomsia A P 2011 *Acta Biomater.* **7** 2355

- [12] Lu H, Zhang T, Wang X P and Fang Q F 2009 *J. Mater. Sci. Mater. Med.* **20** 793
- [13] Allo B A, Rizkalla A S and Mequanint K 2010 *Langmuir* **26** 18340
- [14] Scaffaro R, Re G L, Rigogliuso S and Ghersi G 2012 *Sci. Technol. Adv. Mater.* **13** 45003
- [15] Sepulveda P, Jones J R and Hench L L 2002 *J. Biomed. Mater. Res.* **59** 340
- [16] Hong Y L, Chen X S, Jing X B and Fan H S 2010 *Adv. Mater.* **22** 754
- [17] Fu A, Wilson R J, Smith B R, Mullenix J, Earhart C and Gambhir S S 2012 *ACS Nano.* **6** 6862
- [18] Liu J, Qiao S Z, Hu Q H and Lu G Q 2011 *Small* **7** 425
- [19] Patel D, Kell A, Simard B, Xiang B, Lin H Y and Tian G H 2011 *Biomaterials* **32** 1167
- [20] Ito A, Honda Y K, Kikkawa H, Horiuchi A, Watanabe Y and Kobayashi T 2004 *Cancer Lett.* **212** 167
- [21] Luderer A A, Borrelli N F, Panzarino J N, Mansfield G R and Hess D M 1983 *Radiat. Res.* **94** 190
- [22] Dewey W C 1994 *Int. J. Hyperthermia* **10** 457
- [23] Li X, Wang X P, Hua Z L and Shi J L 2008 *Acta Mater.* **56** 3260
- [24] Zhu Y F, Fang Y and Kaskel S 2010 *J. Phys. Chem.* **114** 16382
- [25] Valdés-Solís T, Rebolledo A F, Sevilla M, Valle-Vigón P, Bomati-Miguel O, Fuertes A B and Tartaj P 2009 *Chem. Mater.* **21** 1806
- [26] Karageorgiou V and Kaplan D P 2005 *Biomaterials* **26** 5474
- [27] Li X, Wang X P, Chen H G and Jiang P 2007 *Chem. Mater.* **19** 4322
- [28] Hadi H, Karbasi S, Hosseinalipour M and Rezaie H R 2010 *J. Mater. Sci. Mater. Med.* **21** 2125
- [29] Peter M, Binulal N S, Nair S V, Selvamurugan N, Tamura H and Jayakumar R 2010 *Chem. Eng. J.* **158** 353
- [30] Costa S, Palenphys E B, Bachmatiuk A, Rummeli M H, Gemming T and Kaleńczukstat R J 2007 *Phys. Status Solidi b* **244** 4315
- [31] Tiainen V M 2001 *Diamond Relat. Mater.* **10** 153
- [32] Low K L, Zein S H S, Tan S H, Phail D S and Boccaccini A R 2011 *Ceram. Int.* **37** 2429
- [33] Madani S Y, Tan A, Dwek M and Seifalian A M 2012 *Int. J. Nanomedicine* **7** 905
- [34] Li X F, Qu F Y and Li W 2012 *J. Sol–Gel Sci. Technol.* **63** 416
- [35] Rámila A, Balas F and Regí M V 2002 *Chem. Mater.* **14** 542
- [36] Regí M V, Arco D and Pariente J P 2000 *J. Biomed. Mater. Res.* **51** 23